

Auto-validating von Neumann Rejection Sampling from Small Phylogenetic Tree Spaces

Raazesh Sainudiin¹ and Thomas York²

¹ Department of Statistics, 1 South Parks Road, University of Oxford,
Oxford OX1 3TG, U.K. sainudii@stats.ox.ac.uk

² Department of Biological Statistics and Computational Biology, Cornell University,
Ithaca, U.S.A. tly2@cornell.edu

Abstract. In phylogenetic inference one is interested in obtaining samples from the posterior distribution over the tree space on the basis of some observed DNA sequence data. The challenge is to obtain samples from this target distribution without any knowledge of the normalizing constant. One of the simplest sampling methods is the rejection sampler due to von Neumann. Here we introduce an auto-validating version of the rejection sampler, via interval analysis, to rigorously draw samples from posterior distributions, based on homologous primate mitochondrial DNA, over small phylogenetic tree spaces.

1 INTRODUCTION

Obtaining samples from a density $p(\theta) \triangleq p^*(\theta)/N_p$, where $\theta \in \Theta$ and Θ is a compact Euclidean subset, *i.e.*, $\Theta \subset \mathbb{R}^n$, without any knowledge of the normalizing constant $N_p \triangleq \int_{\Theta} p^*(\theta) d\theta$, is a basic problem in statistical inference. The usual Monte Carlo methods via conventional floating-point arithmetic are typically non-rigorous. We will concentrate on the rejection sampler due to von Neumann [1] and its rigorous extension for application in phylogenetics. The standard approaches to sampling from the posterior over phylogenies rely on Markov chain Monte Carlo (MCMC) methods. Despite their asymptotic validity, it is nontrivial to guarantee that an MCMC algorithm has converged to stationarity [2], and thus MCMC convergence diagnostics on phylogenetic tree spaces are heuristic [3]. Thus, until now, no rigorous methodology has existed for perfectly sampling from the posterior distribution over phylogenetic tree spaces, even for 3 or 4 taxa. Here, we solve this rigorous posterior sampling problem over small phylogenetic tree spaces.

After a brief introduction to the rejection sampler (RS) in Sect. 2, an interval version of this sampler is formalized in Sect. 3. This sampler is referred to as the Moore rejection sampler (MRS) in honor of Ramon E. Moore who was one of the influential founders of interval analysis [4]. In Sect. 4, we rigorously draw samples from the posterior over small tree spaces. We conclude in Sect. 5. Section 7 summarizes our notation and gives a brief introduction to interval analysis, a prerequisite to understanding MRS. In Sect. 8, Lemma 1 shows that MRS

produces independent samples from the desired target density and Lemma 2 describes the asymptotics of the acceptance probability for a refining family of MRSs. Unlike many conventional samplers, each sample produced by MRS is equivalent to a computer-assisted proof that it is drawn from the desired target, up to the pseudo-randomness of the underlying, deterministic, pseudo-random number generator. An open source C++ class library for MRS is publicly available from www.stats.ox.ac.uk/~sainudii/codes.

2 Rejection Sampler (RS)

Rejection sampling [1] is a Monte Carlo method to draw independent samples from a target probability distribution $p(\theta) \triangleq p^*(\theta)/N_p$, where $\theta \in \Theta \subset \mathbb{R}^n$. Typically the target p is any density that is absolutely continuous with respect to the Lebesgue measure. In most cases of interest we can compute the target shape $p^*(\theta)$ for any $\theta \in \Theta$, but the normalizing constant N_p is unknown. The von Neumann RS can produce samples from p according to Algorithm 1 when provided with (i) a proposal density $q(\theta) = q^*(\theta)/N_q$ from which independent samples can be drawn, $N_q \triangleq \int_{\Theta} q^*(\theta) d\theta$ is known, and $q^*(\theta)$ is computable for any $\theta \in \Theta$ and (ii) a constant c defining the envelope function $f_q(\theta) \triangleq cq^*(\theta)$, such that,

$$f_q(\theta) \triangleq cq^*(\theta) \geq p^*(\theta), \forall \theta \in \Theta . \quad (1)$$

Algorithm 1 von Neumann RS

input: (1) a target shape p^* , (2) a proposal density q , (3) an envelope function f_q and (4) an integer $TRIALS_{MAX}$

output: a sample from U distributed according to p

initialize: $TRIALS \leftarrow 0$, $SUCCESS \leftarrow false$

repeat

 DRAW $T \sim q$ {draw a sample from the random variable T with distribution q }

 DRAW $H \sim Uniform[0, f_q(T)]$, where $f_q(T) \geq p^*(T)$

if $H \leq p^*(T)$ **then**

$U \leftarrow T$, $SUCCESS \leftarrow true$

end if

$TRIALS \leftarrow TRIALS + 1$

until $TRIALS < TRIALS_{MAX}$ or $SUCCESS = true$

U generated by the above algorithm is distributed according to p [5]. Observe that the probability $\mathbf{A}_{f_q}^p$ that a point proposed according to q gets accepted as an independent sample from p through the envelope function f_q is the ratio of the integrals

$$\mathbf{A}_{f_q}^p = \frac{N_p}{N_{f_q}} \triangleq \frac{\int_{\Theta} p^*(\theta) d\theta}{\int_{\Theta} f_q(\theta) d\theta} ,$$

and the probability distribution over the number of samples from q to obtain one sample from p is geometrically distributed with mean $1/\mathbf{A}_{f_q}^p$ [5].

3 Moore Rejection Sampler (MRS)

Moore rejection sampler (MRS) is an auto-validating rejection sampler (RS). It can produce independent samples from any target shape p^* that has a well-defined natural interval extension P^* (Definition 6) over a compact domain Θ . MRS is said to be auto-validating because it automatically obtains a proposal q that is easy to simulate from, and an envelope f_q that is guaranteed to satisfy the envelope condition (1). In summary, the defining characteristics and notations of MRS are:

Compact domain	$\Theta = [\underline{\theta}, \bar{\theta}]$
Target shape	$p^*(\theta) : \Theta \rightarrow \mathbb{R}$
Target integral	$N_p \triangleq \int_{\Theta} p^*(\theta) d\theta$
Target density	$p(\theta) \triangleq \frac{p^*(\theta)}{N_p} : \Theta \rightarrow \mathbb{R}$
Interval extension of p^*	$P^*(\Theta) : \mathbb{I}\Theta \rightarrow \mathbb{I}\mathbb{R}$
Proposal shape	$q^*(\theta) : \Theta \rightarrow \mathbb{R}$
Proposal integral	$N_q \triangleq \int_{\Theta} q^*(\theta) d\theta$
Proposal density	$q(\theta) \triangleq \frac{q^*(\theta)}{N_q} : \Theta \rightarrow \mathbb{R}$
Envelope function	$f_q(\theta) = cq^*(\theta)$
Envelope integral	$N_{f_q} \triangleq \int_{\Theta} f_q(\theta) d\theta = cN_q$
Acceptance probability	$\mathbf{A}_{f_q}^p = \frac{N_p}{N_{f_q}}$
Partition of Θ	$\mathfrak{T} \triangleq \{\Theta^{(1)}, \Theta^{(2)}, \dots, \Theta^{(\mathfrak{T})}\}$.

If $p^* \in \mathfrak{E}$, the class of elementary functions (Definition 8), its natural interval extension P^* is well-defined on Θ and $\mathfrak{T} \triangleq \{\Theta^{(1)}, \Theta^{(2)}, \dots, \Theta^{(|\mathfrak{T}|)}\}$ be a finite partition of Θ , then by Theorem 4 we can enclose $p^*(\Theta^{(i)})$, i.e., the range of p^* over the i -th element of \mathfrak{T} , with the interval extension P^* of p^* .

$$p^*(\Theta^{(i)}) \subseteq P^*(\Theta^{(i)}) \triangleq [\underline{P}^*(\Theta^{(i)}), \bar{P}^*(\Theta^{(i)})], \forall i \in \{1, 2, \dots, |\mathfrak{T}|\}. \quad (2)$$

For the given partition \mathfrak{T} we can construct a partition-specific proposal $q^{\mathfrak{T}}(\theta)$ as a normalized simple function over Θ ,

$$q^{\mathfrak{T}}(\theta) = (N_{q^{\mathfrak{T}}})^{-1} \sum_{i=1}^{|\mathfrak{T}|} \bar{P}^*(\Theta^{(i)}) \mathbf{1}_{\{\theta \in \Theta^{(i)}\}}, \quad (3)$$

with the normalizing constant $N_{q^{\mathfrak{T}}} \triangleq \sum_{i=1}^{|\mathfrak{T}|} \left(d(\Theta^{(i)}) \cdot \bar{P}^*(\Theta^{(i)}) \right)$, where, $d(\Theta) = d([\underline{\theta}, \bar{\theta}]) = \bar{\theta} - \underline{\theta}$ is the *diameter* of Θ . The next ingredient $f_{q^{\mathfrak{T}}}(\theta)$ for our rejection sampler can simply be

$$f_{q^{\mathfrak{T}}}(\theta) = \sum_{i=1}^{|\mathfrak{T}|} \bar{P}^*(\Theta^{(i)}) \mathbf{1}_{\{\theta \in \Theta^{(i)}\}}. \quad (4)$$

The necessary envelope condition (1) is satisfied by $f_{q^{\mathfrak{T}}}(\theta)$ because of (2). Now, we have all the ingredients to perform a more efficient partition-specific Moore

rejection sampling. Lemma 1 shows that if the target shape p^* has a well-defined natural interval extension P^* , and if U is generated according to Algorithm 1, and if the proposal density $q^{\mathfrak{I}}(\theta)$ and the envelope function $f_{q^{\mathfrak{I}}}(\theta)$ are given by (3) and (4), respectively, then U is distributed according to the target p . Note that the above arguments as well as those in the proof of Lemma 1 naturally extend when $\Theta \subset \mathbb{R}^n$ for $n > 1$. In the multivariate case, $\Theta^{(i)} \in \mathbb{I}\mathbb{R}^n$ (Definition 4) is a box. Thus, we naturally replace the diameter of an interval by the *volume* of a box $v(\Theta^{(i)}) \triangleq \prod_{k=1}^n d(\Theta_k^i)$. The envelopes and proposals are now simple functions over a partition of the domain into boxes. Analogous to the univariate case, the accepted samples are uniformly distributed in the region $S \subset \mathbb{R}^{n+1}$ ‘under’ p^* and ‘over’ Θ . Hence their density is p [5].

Next we bound the acceptance probability $\mathbf{A}_{f_{q^{\mathfrak{I}}}}^p \triangleq \mathbf{A}_{\mathfrak{I}}^p$ for this sampler. Due to the linearity of the integral operator and (2),

$$\begin{aligned} N_p &\triangleq \int_{\Theta} p^*(\theta) d\theta \\ &= \sum_{i=1}^{|\mathfrak{I}|} \int_{\Theta^{(i)}} p^*(\theta) d\theta \\ &\in \sum_{i=1}^{|\mathfrak{I}|} (d(\Theta^{(i)}) \cdot P^*(\Theta^{(i)})) \\ &= [\sum_{i=1}^{|\mathfrak{I}|} (d(\Theta^{(i)}) \cdot \underline{P}^*(\Theta^{(i)})), \sum_{i=1}^{|\mathfrak{I}|} (d(\Theta^{(i)}) \cdot \overline{P}^*(\Theta^{(i)}))] . \end{aligned}$$

Therefore,

$$\mathbf{A}_{\mathfrak{I}}^p = \frac{N_p}{N_{f_{q^{\mathfrak{I}}}}} = \frac{N_p}{\sum_{i=1}^{|\mathfrak{I}|} (d(\Theta^{(i)}) \cdot \overline{P}^*(\Theta^{(i)}))} \geq \frac{\sum_{i=1}^{|\mathfrak{I}|} (d(\Theta^{(i)}) \cdot \underline{P}^*(\Theta^{(i)}))}{\sum_{i=1}^{|\mathfrak{I}|} (d(\Theta^{(i)}) \cdot \overline{P}^*(\Theta^{(i)}))} .$$

If $p^* \in \mathfrak{E}_{\mathfrak{I}}$, the Lipschitz class of elementary functions (Definition 10), then we might expect the enclosure of N_p to be proportional to the mesh $w \triangleq \max_{i \in \{1, \dots, |\mathfrak{I}|\}} d(\Theta^{(i)})$ of the partition \mathfrak{I} . Lemma 2 shows that if $p^* \in \mathfrak{E}_{\mathfrak{I}}$ and \mathfrak{U}_W is a uniform partition of Θ into W intervals, then the acceptance probability $\mathbf{A}_{\mathfrak{U}_W}^p = 1 - \mathcal{O}(1/W)$. Thus, the acceptance probability approaches 1 at a rate that is no slower than linearly with the mesh. We can gain geometric insight into the sampler from an example. The dashed lines of a given shade, depicting a simple function in Fig. 6, is a partition-specific envelope function (4) for the target shape $s^*(x) = -\sum_{k=1}^5 kx \sin(\frac{k(x-3)}{3})$ over the domain $\Theta = [-10, 6]$ and its normalization gives the corresponding proposal function (3). As the refinement of Θ proceeds through uniform bisections, the partition size increases as 2^i , $i = 1, 2, 3, 4$. Each of the corresponding envelope functions in increasing shades of gray can be used to draw auto-validated samples from the target $s(x)$ over Θ . Note how the acceptance probability (ratio of the area below the target shape to that below the envelope) increases with refinement.

We studied the efficiency of uniform partitions for their mathematical tractability. In practice, we may further increase the acceptance probability for a given partition size by adaptively partitioning Θ . In our context, adaptive means the possible exploitation of any current information about the target. We can refine the current partition \mathfrak{I}_{α} and obtain a finer partition $\mathfrak{I}_{\alpha'}$ with an additional box by bisecting a box $\Theta^{(*)} \in \mathfrak{I}_{\alpha}$ along the side with the maximal diameter. There

are several ways to choose a $\Theta^{(*)} \in \mathfrak{T}_\alpha$ for bisection. When $\Theta^{(i)} \in \mathbb{I}\mathbb{R}^n$ has volume $v(\Theta^{(i)})$, an optimal choice for $\Theta^{(*)} = \arg \max_{\Theta^{(i)} \in \mathfrak{T}_\alpha} (v(\Theta^{(i)}) \cdot d(P^*(\Theta^{(i)})))$. Under this partitioning scheme, we employ a priority queue to conduct sequential refinements of Θ . This approach avoids the exhaustive $\arg \max$ computations to obtain the $\Theta^{(*)}$ for bisection at each refinement step. Once we have any partition \mathfrak{T} of Θ , we can efficiently sample $\theta \sim q^\mathfrak{T}$ given by (3) in two steps. First we sample a box $\Theta^{(i)} \in \mathfrak{T}$ according to the discrete distribution $t(\Theta^{(i)})$,

$$t(\Theta^{(i)}) = \frac{v(\Theta^{(i)}) \cdot \overline{P^*}(\Theta^{(i)})}{\sum_{i=1}^{|\mathfrak{T}|} v(\Theta^{(i)}) \cdot \overline{P^*}(\Theta^{(i)})}, \quad \Theta^{(i)} \in \mathfrak{T}, \quad (5)$$

and then we choose a $\theta \in \Theta^{(i)}$ uniformly at random. Sampling from large discrete distributions (with million states or more) can be made faster by preprocessing the probabilities and saving the result in some convenient lookup table. This basic idea [6] allows samples to be drawn rapidly. We employ a more efficient preprocessing strategy [7] that allows samples to be drawn in constant time even for very large discrete distributions as implemented in the GNU Scientific Library [8]. Thus, by means of priority queues and lookup tables we can efficiently manage our adaptive partitioning of the domain for envelope construction, and rapidly draw samples from the proposal distribution. We used the Mersenne Twister random number generator [9] in this paper. Our sampler class builds on C-XSC 2.0, a C++ class library for extended scientific computing using interval methods [10]. All computations were done on a 2.8 GHz Pentium IV machine with 1GB RAM. Having given theoretical and practical considerations to our Moore rejection sampler, we are ready to draw samples from various targets.

4 Auto-validating Independent Posterior Samples from Triplets and Quartets

Inferring the ancestral relationship among a set of species based on their DNA sequences is a basic problem in phylogenetics [11]. One can obtain the likelihood of a particular phylogenetic tree that relates the species of interest by superimposing a simple Markov model of DNA substitution due to Jukes and Cantor [12] on that tree. The length of an edge (branch length) connecting two nodes (species) in the tree represents the amount of evolutionary time (divergence) between the two species. The likelihood function over trees obtained through a post-order traversal (e.g. [13]) has a natural interval extension over boxes of trees [14]. This allows us to draw samples from the posterior distribution over a compact box specified by our prior distribution on the tree space using our MRS. We assume a uniform prior over the possible unrooted topologies and a uniform product prior over all branch lengths in the range $[10^{-10}, 10]$. We consider two mitochondrial DNA data sets.

4.1 Chimpanzee, Gorilla, Orangutan and Gibbon

Our posterior distribution is based on the data from an 895 bp long homologous segment of mitochondrial DNA from chimpanzee, gorilla, orangutan, and

gibbon, containing the genes for three transfer RNAs and parts of two proteins [15]. Under the assumption of independence across sites, the sufficient statistics only comprise of the distinct site patterns and their counts. The data for chimpanzee, gorilla and orangutan can be summarized by the following 29 distinct site patterns and counts:

```

site      :                               1 1 1 1 1 1 1 1 1 1 2 2 2 2 2 2 2 2 2
pattern   : 1 2 3 4 5 6 7 8 9 0 1 2 3 4 5 6 7 8 9 0 1 2 3 4 5 6 7 8 9
. . . . .
chimpanzee : a g c t a t c a c c c a t c t g c c g t a c t a a g c g t
gorilla    : a g c t g t t a t c a a c a c g c a a a a t c c g g t a t
orangutan  : a g c t a c c g t t c c c a t a a t a a t a a a g c g c a
. . . . .
site      : 2 7 2 1 1 3 1 1 9 2 1 8 2 3 1 8 7 1 9 2 4 2 1 2 1 1 2 1 3
pattern   : 3 1 2 6 3 1 6 8 0 2 0
counts    : 2 9 8

```

In the above data set, the first column (1.aaa.232) expresses that there are 232 site patterns with nucleotide ‘a’ in all three species, ..., and the last column (29.tta.3) expresses that there are 3 site patterns with nucleotide ‘t’ in chimpanzee and gorilla, and nucleotide ‘a’ in orangutan. The data for all four primates can be summarized by 61 distinct site patterns as parsed in [14]. 10000 independent samples were drawn in 942 CPU seconds from the posterior distribution over Jukes-Cantor triplets, i.e. unrooted trees with three edges corresponding to the three primates emanating from their common ancestor. Figure 1 shows these samples (blue dots) scattered about the verified global maximum likelihood estimate (MLE) of the triplet obtained in [14] and subsequently confirmed algebraically in [16]. We also drew 10000 independent samples from the posterior based on the 198 tRNA-coding DNA sites (green dots in Fig. 1) as well as from that based on the remaining 697 protein-coding sites (red dots in Fig. 1). The former posterior samples, corresponding to the tRNA-coding sites, are more dispersed than the posterior samples based on the entire sequence. This is due to the smaller number of tRNA-coding sites making the posterior less concentrated. We were able to reject the null hypothesis of homogeneity between the posterior samples based on the tRNA-coding sites and that based on the protein-coding sites at the 10% significance level (P-value = 0.06 from a non-parametric bootstrap of Hotelling’s trace statistic based on 100 random permutations of the sites). Any biological interpretation of this test must be done cautiously since the Jukes and Cantor model employed here forbids any transition:transversion bias that is reportedly relevant for this data [15].

[Fig. 1 about here.]

We were able to draw samples from Jukes-Cantor quartets by adding the homologous sequence of the Gibbon. Now, the problem is a more challenging because there are three distinct tree topologies in the unrooted, bifurcating, quartet tree space, and each of these topologies has five edges. Thus, the domain of quartets is a piecewise Euclidean space that arises from a fusion of 3 distinct five

dimensional orthants. Since the post-order traversals specifying the likelihood function are topology-specific, we extended the likelihood over a compact box of quartets in a topology-specific manner. The computational time was about a day and a half to draw 10000 samples from the quartet target due to low acceptance probability of the naive likelihood function based on the 61 distinct site patterns. All the samples had the topology which grouped Chimp and Gorilla together, i.e. ((Chimp, Gorilla), (Orangutan, Gibbon)). The samples were again scattered about the verified global MLE of the quartet [14]. The marginal triplet trees (gray dots) within the sampled quartets are depicted in Fig. 2. This quartet likelihood function has an elaborate DAG (Definition 9) with numerous operations. When the data got compressed into sufficient statistics through algebraic statistical methods [17], the efficiency increased tremendously (e.g. for triplets the efficiency increases by a factor of 3.7). This is due to the number of leaf nodes in the target DAG, which encode the distinct site patterns of the observed data into the likelihood function, getting reduced from 29 to 5 for the triplet target and from 61 to 15 for the quartet target [17]. Poor sampler efficiency makes it currently impractical to sample from trees with five leaves and 15 topologies (see Sect. 5 for a discussion on improvements). However, one could use such triplets and quartets drawn from the posterior distribution to stochastically amalgamate and produce estimates of larger trees via fast amalgamating algorithms [18, 19], which may then be used to combat the slow mixing in MCMC methods [3] by providing a good set of initial trees.

[Fig. 2 about here.]

4.2 Neandertal, Human and Chimpanzee

We used the whole mitochondrial genome shotgun sequence (gi|115069275) of a Neandertal fossil Vi-80, from Vindija cave, Croatia [20], and its homologous sequence in a human (gi|13273200) and a chimpanzee (gi|1262390), as summarized by the 15 sufficient site patterns and their counts below, to conduct statistical inference about the human-neandertal divergence time.

```

site      :           1 1 1 1 1 1
pattern   : 1 2 3 4 5 6 7 8 9 0 1 2 3 4 5
. . . . .
neandertal : t t c a g g t g t c a a c a a
human      : t t c a g g t a c c a g t a g
chimpanzee : t c c a g a a a t t g a c t g
. . . . .
site      : 6 1 6 6 4 1 2 1 2 1 1 1 1 1 1
pattern   : 0 4 0 8 5 0           4 5
counts    : 5   3 5 0

```

We drew 10000 auto-validating independent samples from each of three posterior distributions; (1) over the space of unrooted triplets under the Jukes-Cantor model in 312 CPU seconds, (2) over the clocked and rooted triplets under a

Jukes-Cantor model in 375 CPU seconds and (3) over the clocked and rooted triplets under a more general mutational model due to Hasegawa, Kishino and Yano (HKY) [21] in 1.2 CPU hours. In the HKY model we used the empirical nucleotide frequencies from the data ($\pi_T = 0.2588$, $\pi_C = 0.2571$, $\pi_A = 0.2916$, $\pi_G = 0.1925$) and a hominid-specific transition/transversion rate of 2.0. Unlike the Jukes-Cantor model, all 15 distinct site patterns are minimally sufficient under the HKY model and this is reflected in its longer CPU time. Both models gave similar posterior samples over rooted triplets, as shown in Fig. 3.

[Fig. 3 about here.]

We transformed the three posterior distributions over the triplet spaces; (1) unrooted Jukes-Cantor triplets that were rooted using the mid-point rooting method, (2) rooted Jukes-Cantor triplets and (3) rooted HKY triplets, respectively, into three posterior distributions over the human-neandertal divergence time relative to the human-chimp divergence time (Fig. 4). The corresponding posterior quantiles ($\{5\%, 50\%, 95\%\}$) for the human-neandertal divergence times are $\{0.0643, 0.125, 0.214\}$, $\{0.0694, 0.142, 0.263\}$ and $\{0.0682, 0.143, 0.268\}$, respectively. We constrained the neandertal lineage to be a fraction of the human lineage in branch length in order to estimate the age of the neandertal fossil from the rooted HKY triplets. The posterior quantiles of the fossil date in units of human-chimp divergence is $\{0.00685, 0.0666, 0.195\}$. The estimate of 38,310 years based on carbon-14 accelerator mass spectrometry [20] is within our $[5\%, 95\%]$ posterior quantile interval for the fossil date, provided the human-chimp divergence estimates ranges in $[196103, 5.6 \times 10^6]$. Thus, reasonable bounds for the human-chimp divergence are 4×10^6 and 5.6×10^6 years. Based on these calendar year estimates, we transformed the posterior quantiles of the human-neandertal divergence times from the rooted HKY triplets into $\{272680, 571124, 1073375\}$ and $\{381752, 799574, 1502724\}$, respectively. Our $[5\%, 95\%]$ posterior intervals contain the interval estimate of $[461000, 825000]$ years reported in [20]. However, our confidence intervals are from perfectly independent samples from the posterior and account for the finite number of neandertal sites that were successfully sequenced, unlike those obtained on the basis of a bootstrap of site patterns [22] or heuristic MCMC [2]. Unfortunately, our human-neandertal divergence estimates are overestimates as they ignore the non-negligible time to coalescence of the human and neandertal homologs within the human-neandertal ancestral population. Improvements to our estimates based on the other 310 human and 4 chimpanzee homologs reported in [20] may be possible with more sophisticated models of populations within a phylogeny and need further investigation.

[Fig. 4 about here.]

5 Conclusion

Interval methods provide for a rigorous sampling from posterior target densities over small phylogenetic tree spaces. When one substitutes conventional floating-

point arithmetic for real arithmetic in a computer and uses discrete lattices to construct the envelope and/or proposal, it is generally not possible to guarantee the envelope property, and thereby ensure that samples are drawn from the desired target density, except in special cases [23]. Thus, the construction of the Moore rejection sampler through interval methods, that enclose the target shape over the entire real continuum in any box of the domain with machine-representable bounds, in a manner that rigorously accounts for all sources of numerical errors (see [24] for a discussion on error control), naturally guarantees that the Moore rejection samples are independent draws from the desired target. Moreover, the target is allowed to be multivariate and/or non-log-concave with possibly ‘pathological’ behavior, as long as it has a well-defined interval extension.

The efficiency of MRS is not immune to the curse of dimensionality and target DAG complexity. When the DAG for the likelihood gets large, its natural interval extension can have terrible over-enclosures of the true range, which in turn forces the adaptive refinement of the domain to be extremely fine for efficient envelope construction. Thus, a naive application of interval methods to targets with large DAGs can be terribly inefficient. In such cases, sampler efficiency rather than rigor is the issue. Thus, one may fail to obtain samples in a reasonable time, rather than (as may happen with non-rigorous methods) produce samples from some unknown and undesired target. There are several ways in which efficiency can be improved for such cases. First, the particular structure of the target DAG should be exploited to avoid any redundant computations. For example, algebraic statistical methods can be used to find sufficient statistics to dissolve symmetries in the DAG as done in Sect. 4. Second, we can further improve efficiency by limiting ourselves to differentiable targets in C^n . Tighter enclosures of the range $p^*(\Theta^{(i)})$ with $P^*(\Theta^{(i)})$ can come from the enclosures of Taylor expansions of p^* around the midpoint $m(\Theta^{(i)})$ through interval-extended automatic differentiation (see [24]) that can then yield tighter estimates of the integral enclosures [25]. Third, we can employ pre-processing to improve efficiency. For example, we can pre-enclose the range of a possibly rescaled p^* over a partition of the domain and then obtain the enclosure of P^* over some arbitrary Θ through a combination of hash access and hull operations on the pre-enclosures. Such a pre-enclosing technique reduces not only the overestimation of target shapes with large DAGs but also the computational cost incurred while performing interval operations with processors that are optimized for floating-point arithmetic. Fourth, efficiency at the possible cost of rigor can also be gained (up to 30%) by foregoing directed rounding during envelope construction.

6 Acknowledgments

This was supported by a joint NSF/NIGMS grant DMS-02-01037. R.S. is a Research Fellow of the Royal Commission for the Exhibition of 1851. Many thanks to Rob Strawderman and Warwick Tucker for constructive comments on

the sampler and Jo Felsenstein for clarifying the transition probabilities under the HKY model.

7 Appendix A

Definition 1. Let $X \triangleq [\underline{x}, \bar{x}]$ be an interval in $\mathbb{IR} \triangleq \{[\underline{x}, \bar{x}] : \underline{x} \leq \bar{x}, \underline{x}, \bar{x} \in \mathbb{R}\}$

Definition 2 (Interval arithmetic). If the binary operator \star is one of the elementary arithmetic operations $\{+, -, \cdot, /\}$, then we define an arithmetic on operands in \mathbb{IR} by

$$X \star Y \triangleq \{x \star y : x \in X, y \in Y\}$$

with the exception that X/Y is undefined if $0 \in Y$.

Theorem 1. Arithmetic on the pair $X, Y \in \mathbb{IR}$ is given by:

$$\begin{aligned} X + Y &= [\underline{x} + \underline{y}, \bar{x} + \bar{y}] \\ X - Y &= [\underline{x} - \bar{y}, \bar{x} - \underline{y}] \\ X \cdot Y &= [\min\{\underline{x}\underline{y}, \underline{x}\bar{y}, \bar{x}\underline{y}, \bar{x}\bar{y}\}, \max\{\underline{x}\underline{y}, \underline{x}\bar{y}, \bar{x}\underline{y}, \bar{x}\bar{y}\}], \\ X/Y &= X \cdot [1/\bar{y}, 1/\underline{y}], \text{ provided, } 0 \notin Y. \end{aligned}$$

Proof (cf. [25]): Since any real arithmetic operation $x \star y$, where $\star \in \{+, -, \cdot, /\}$ and $x, y \in \mathbb{R}$, is a continuous function $x \star y \triangleq \star(x, y) : \mathbb{R} \times \mathbb{R} \rightarrow \mathbb{R}$, except when $y = 0$ under $/$ operation. Since X and Y are simply connected compact intervals, so is their product $X \times Y$. On such a domain $X \times Y$, the continuity of $\star(x, y)$ (except when $\star = /$ and $0 \in Y$) ensures the attainment of a minimum, a maximum and all intermediate values. Therefore, with the exception of the case when $\star = /$ and $0 \in Y$, the range $X \star Y$ has an interval form $[\min(x \star y), \max(x \star y)]$, where the min and max are taken over all pairs $(x, y) \in X \times Y$. Fortunately, we do not have to evaluate $x \star y$ over every $(x, y) \in X \times Y$ to find the global min and global max of $\star(x, y)$ over $X \times Y$, because the monotonicity of the $\star(x, y^*)$ in terms of $x \in X$ for any fixed $y^* \in Y$ implies that the extremal values are attained on the boundary of $X \times Y$, i.e., the set $\{\underline{x}, \underline{y}, \bar{x}, \bar{y}\}$. Thus the theorem can be verified by examining the finitely many boundary cases. \square

An extremely useful property of interval arithmetic that is a direct consequence of Definition 2 is summarized by the following theorem.

Theorem 2 (Fundamental property of interval arithmetic). If $X \subseteq X'$ and $Y \subseteq Y'$ and $\star \in \{+, -, \cdot, /\}$, then

$$X \star Y \subseteq X' \star Y',$$

where we require that $0 \notin Y'$ when $\star = /$.

Proof:

$$X \star Y = \{x \star y : x \in X, y \in Y\} \subseteq \{x \star y : x \in X', y \in Y'\} = X' \star Y'. \square$$

Note that an immediate implication of Theorem 2 is that when $X = x$ and $Y = y$ are thin intervals (real numbers x and y), then $X' \star Y'$ will contain the result of the real arithmetic operation $x \star y$.

Definition 3 (Range). Consider a real-valued function $f : D \rightarrow \mathbb{R}$ where the domain $D \subseteq \mathbb{R}^n$. The range of f over any $E \subseteq D$ is represented by $Rng(f; E)$ and defined to be the set

$$Rng(f; E) \triangleq \{f(x) : x \in E\}$$

However, when the range of f over any $X \in \mathbb{IR}^n$ such that $X \subseteq D$ is of interest, we will use the short-hand $f(X)$ for $Rng(f; X)$.

Definition 4 (Interval extension of subsets of \mathbb{R}^n). For any Euclidean subset $\Theta \subseteq \mathbb{R}^n$ let us denote its interval extension by $\mathbb{I}\Theta$ and define it to be the set

$$\mathbb{I}\Theta \triangleq \{X \in \mathbb{IR}^n : \underline{x}, \bar{x} \in \Theta\}$$

We refer the the k th interval of interval vector or box $X \in \mathbb{IR}^n$ by X_k .

Definition 5 (Inclusion isotony). An box-valued map $F : D \rightarrow \mathbb{IR}^m$, where $D \in \mathbb{IR}^n$, is inclusion isotonic if it satisfies the property

$$\forall X \subseteq Y \subseteq D \implies F(X) \subseteq F(Y).$$

Definition 6 (The natural interval extension). Consider a real-valued function $f : D \rightarrow \mathbb{R}$ given by a formula, where the domain $D \in \mathbb{IR}^n$. If real constants, variables, and operations in f are replaced by their interval counterparts, then one obtains

$$F(X) : \mathbb{I}D \rightarrow \mathbb{IR}.$$

F is known as the natural interval extension of f . This extension is well-defined if we do not run into division by zero.

Theorem 3 (Inclusion isotony of rational functions). Consider the rational function $f(x) = p(x)/q(x)$, where p and q are polynomials. Let F be its natural interval extension such that $F(Y)$ is well-defined for some $Y \in \mathbb{IR}$ and let $X, X' \in \mathbb{IR}$. Then we have

- (i) Inclusion isotony: $\forall X \subseteq X' \subseteq Y \implies F(X) \subseteq F(X')$, and
- (ii) Range enclosure: $\forall X \subseteq Y \implies Rng(f; X) = f(X) \subseteq F(X)$.

Proof (cf. [25]): Since $F(Y)$ is well-defined, we will not run into division by zero, and therefore (i) follows from the repeated invocation of Theorem 2. We can prove (ii) by contradiction. Suppose $Rng(f; X) \not\subseteq F(X)$. Then there exists $x \in X$, such that $f(x) \in Rng(f; X)$ but $f(x) \notin F(X)$. This in turn implies that $f(x) = F([x, x]) \notin F(X)$, which contradicts (i). Therefore, our supposition cannot be true and we have proved (ii) $Rng(f; X) \subseteq F(X)$. \square

Definition 7 (Standard functions). Piece-wise monotone functions, including exponential, logarithm, rational power, absolute value, and trigonometric functions, constitute the set of standard functions

$$\mathfrak{S} = \{a^x, \log_b(x), x^{p/q}, |x|, \sin(x), \cos(x), \tan(x), \sinh(x), \dots, \arcsin(x), \dots\}.$$

Such functions have well-defined interval extensions that satisfy inclusion isotony and *exact range enclosure*, i.e., $Rng(f; X) = f(X) = F(X)$. Consider the following definitions for the interval extensions for some monotone functions in \mathfrak{S} with $X \in \mathbb{IR}$,

$$\begin{aligned} \exp(X) &= [\exp(\underline{x}), \exp(\overline{x})] \\ \arctan(X) &= [\arctan(\underline{x}), \arctan(\overline{x})] \\ \sqrt{\overline{(X)}} &= [\sqrt{\underline{(x)}}, \sqrt{\overline{(x)}}] && \text{if } 0 \leq \underline{x} \\ \log(X) &= [\log(\underline{x}), \log(\overline{x})] && \text{if } 0 < \underline{x} \end{aligned}$$

and a piece-wise monotone function in \mathfrak{S} with \mathbb{Z}^+ and \mathbb{Z}^- representing the set of positive and negative integers, respectively.

$$X^n = \begin{cases} [\underline{x}^n, \overline{x}^n] & : \text{if } n \in \mathbb{Z}^+ \text{ is odd,} \\ [(\underline{X})^n, |\overline{X}|^n] & : \text{if } n \in \mathbb{Z}^+ \text{ is even,} \\ [1, 1] & : \text{if } n = 0, \\ [1/\overline{x}, 1/\underline{x}]^{-n} & : \text{if } n \in \mathbb{Z}^-; 0 \notin X \end{cases}$$

Definition 8 (Elementary functions). *A real-valued function that can be expressed as a finite combination of constants, variables, arithmetic operations, standard functions and compositions is called an elementary function. The set of all such elementary functions is referred to as \mathfrak{E} .*

Definition 9 (Directed acyclic graph (DAG) of a function). *One can think of the process by which an elementary function f is computed as the result of a sequence of recursive operations with the subexpressions f_i of f where, $i = 1, \dots, n < \infty$. This involves the evaluation of the subexpression f_i at node i with operands s_{i_1}, s_{i_2} from the sub-terminal nodes of i given by the directed acyclic graph (DAG) for f*

$$s_i = \odot f_i \triangleq \begin{cases} f_i(s_{i_1}, s_{i_2}) & : \text{if node } i \text{ has 2 sub-terminal nodes } s_{i_1}, s_{i_2} \\ f_i(s_{i_1}) & : \text{if node } i \text{ has 1 sub-terminal node } s_{i_1} \\ I(s_i) & : \text{if node } i \text{ is a leaf or terminal node, } I(x) = x. \end{cases} \quad (6)$$

The leaf or terminal node of the DAG is a constant or a variable and thus the f_i for a leaf i is set equal to the respective constant or variable. The recursion starts at the leaves and terminates at the root of the DAG. The DAG for an elementary f with n sub-expressions f_1, f_2, \dots, f_n is :

$$\{\odot f_i\}_{i=1}^n \rightsquigarrow \odot f_n = f(x), \quad (7)$$

where each $\odot f_i$ is computed according to (6).

For example the elementary function $x \cdot \sin((x - 3)/3)$ can be obtained from the terminus $\odot f_6$ of the recursion $\{\odot f_i\}_{i=1}^6$ on the DAG for f as shown in Fig. 5.

[Fig. 5 about here.]

It would be convenient if guaranteed enclosures of the range $f(X)$ of an elementary f can be obtained by its natural interval extension $F(X)$. We show that inclusion isotony does indeed hold for F , i.e. if $X \subseteq Y$, then $F(X) \subseteq F(Y)$, and in particular, the *inclusion property* that $x \in X \implies f(x) \in F(X)$ does hold.

Theorem 4 (The fundamental theorem of interval analysis). *Consider any elementary function $f \in \mathfrak{E}$. Let $F : Y \rightarrow \mathbb{IR}$ be its natural interval extension such that $F(Y)$ is well-defined for some $Y \in \mathbb{IR}$ and let $X, X' \in \mathbb{IR}$. Then we have*

- (i) Inclusion isotony: $\forall X \subseteq X' \subseteq Y \implies F(X) \subseteq F(X')$, and
- (ii) Range enclosure: $\forall X \subseteq Y \implies \text{Rng}(f; X) = f(X) \subseteq F(X)$.

Proof (cf. [25]): Any elementary function $f \in \mathfrak{E}$ is defined by the recursion 7 on its sub-expressions f_i where $i \in \{1, \dots, n\}$ according to its DAG. If $f(x) = p(x)/q(x)$ is a rational function, then the theorem already holds by Theorem 3, and if $f \in \mathfrak{S}$ then the theorem holds because the range enclosure is exact for standard functions. Thus it suffices to show that if the theorem holds for $f_1, f_2 \in \mathfrak{E}$, then the theorem also holds for $f_1 \star f_2$, where $\star \in \{+, -, /, \cdot, \circ\}$. By \circ we mean the composition operator. Since the proof is analogous for all five operators, we only focus on the \circ operator. Since F is well-defined on its domain Y , neither the real-valued f nor any of its sub-expressions f_i have singularities in its respective domain Y_i induced by Y . In particular f_2 is continuous on any X_2 and X'_2 such that $X_2 \subseteq X'_2 \subseteq Y_2$ implying the compactness of $F_2(X_2) \triangleq W_2$ and $F_2(X'_2) \triangleq W'_2$, respectively. By our assumption that F_1 and F_2 are inclusion isotonic we have that $W_2 \subseteq W'_2$ and also that

$$F_1 \circ F_2(X_2) = F_1(F_2(X_2)) = F_1(W_2) \subseteq F_1(W'_2) = F_1(F_2(X'_2)) = F_1 \circ F_2(X'_2)$$

The range enclosure is a consequence of inclusion isotony by an argument identical to that given in the proof for Theorem 3. \square

The fundamental implication of the above theorem is that it allows us to enclose the range of any elementary function and thereby produces an upper bound for the global maximum and a lower bound for the global minimum over any compact subset of the domain upon which the function is well-defined. We will see in the sequel that this is the work-horse of randomized enclosure algorithms that efficiently produce samples even from highly multi-modal target distributions.

Unlike the natural interval extension of an $f \in \mathfrak{S}$ that produces exact range enclosures, the natural interval extension $F(X)$ of an $f \in \mathfrak{E}$ often overestimates the range $f(X)$, but can be shown under mild conditions to linearly approach the range as the maximal diameter of the box X goes to zero, i.e., $\mathfrak{h}(F(X), f(X)) \leq \alpha \cdot d_\infty(X) \triangleq \max_i d(X_i)$ for some $\alpha \geq 0$. This implies that a partition of X into smaller boxes $\{X^{(1)}, \dots, X^{(m)}\}$ gives better enclosures of $f(X)$ through the union $\bigcup_{i=1}^m F(X^{(i)})$ as illustrated in Fig. 6. Next we make the above statements precise.

[Fig. 6 about here.]

Definition 10. A function $f : D \rightarrow \mathbb{R}$ is Lipschitz if there exists a Lipschitz constant K such that, for all $x, y \in D$, we have $|f(x) - f(y)| \leq K|x - y|$. We define $\mathfrak{E}_{\mathfrak{L}}$ to be the set of elementary functions whose sub-expressions f_i , $i = 1, \dots, n$ at the nodes of the corresponding DAGs are all Lipschitz.

Theorem 5 (Range enclosure tightens linearly with mesh). Consider a function $f : D \rightarrow \mathbb{R}$ with $f \in \mathfrak{E}_{\mathfrak{L}}$. Let F be an inclusion isotonic interval extension of f such that $F(X)$ is well-defined for some $X \in \mathbb{IR}, X \subseteq I$. Then there exists a positive real number K , depending on F and X , such that if $X = \cup_{i=1}^k X^{(i)}$, then

$$\text{Rng}(f; X) \subseteq \bigcup_{i=1}^k F(X^{(i)}) \subseteq F(X)$$

and

$$r\left(\bigcup_{i=1}^k F(X^{(i)})\right) \leq r(\text{Rng}(f; X)) + K \max_{i=1, \dots, k} r(X^{(i)})$$

Proof : The proof is given by an induction on the DAG for f similar to the proof of Theorem 4 (See [25]).

8 Appendix B

Here we will study the Moore rejection sampler (MRS) carefully. Lemma 1 shows that MRS indeed produces independent samples from the desired target and Lemma 2 describes the asymptotics of the acceptance probability as the partition of the domain is refined.

Lemma 1. Suppose that the target shape p^* has a well-defined natural interval extension P^* . If U is generated according to Algorithm 1, and if the proposal density $q^{\mathfrak{I}}(\theta)$ and the envelope function $f_{q^{\mathfrak{I}}}(\theta)$ are given by (3) and (4), respectively, then U is distributed according to the target p .

Proof: From (3) and (4) observe that $f_{q^{\mathfrak{I}}}(t) = q^{\mathfrak{I}}(t)N_{q^{\mathfrak{I}}}$. Let us define the following two subsets of \mathbb{R}^2 ,

$$\mathcal{B}_q = \{(t, h) : 0 \leq h \leq f_{q^{\mathfrak{I}}}(t)\}, \text{ and } \mathcal{B}_p = \{(t, h) : 0 \leq h \leq p^*(t)\}.$$

First let us agree that Algorithm 1 produces a pair (T, H) that is uniformly distributed on \mathcal{B}_q . We can see this by letting $k(t, h)$ denote the joint density of (T, H) and $k(h|t)$ denote the conditional density of H given $T = t$. Then,

$$k(t, h) = \begin{cases} q^{\mathfrak{I}}(t) k(h|t) & \text{if } (t, h) \in \mathcal{B}_q \\ 0 & \text{otherwise .} \end{cases}$$

Since we sample a uniform height h for a given t ,

$$k(h|t) = \begin{cases} (f_{q^{\mathfrak{I}}}(t))^{-1} = (q^{\mathfrak{I}}(t)N_{q^{\mathfrak{I}}})^{-1} & \text{if } h \in [0, f_{q^{\mathfrak{I}}}(t)] \\ 0 & \text{otherwise.} \end{cases}$$

Therefore,

$$k(t, h) = \begin{cases} q^{\mathfrak{z}}(t) k(h|t) = q^{\mathfrak{z}}(t)/(q^{\mathfrak{z}}(t) N_{q^{\mathfrak{z}}}) = (N_{q^{\mathfrak{z}}})^{-1} & \text{if } (t, h) \in \mathcal{B}_q \\ 0 & \text{otherwise .} \end{cases}$$

Thus we have shown that the joint density of (T, H) is a uniformly distribution on \mathcal{B}_q . The above relationship also makes geometric sense since the volume of \mathcal{B}_q is exactly $N_{q^{\mathfrak{z}}}$. Now, let (T^*, H^*) be an accepted point, i.e., $(T^*, H^*) \in \mathcal{B}_p \subseteq \mathcal{B}_q$. Then, the uniform distribution of (T, H) on \mathcal{B}_q implies the uniform distribution of (T^*, H^*) on \mathcal{B}_p . Since the volume of \mathcal{B}_p is N_p , the p.d.f. of (T^*, H^*) is identically $1/N_p$ on \mathcal{B}_p and 0 elsewhere. Hence, the marginal p.d.f. of $U = T^*$ is

$$\begin{aligned} w(u) &= \int_0^{p^*(u)} 1/N_p dh \\ &= 1/N_p \int_0^{p^*(u)} 1 dh \\ &= 1/N_p \int_0^{N_p p(u)} 1 dh, \quad \because p(u) = p^*(u)/N_p \\ &= p(u). \quad \square \end{aligned}$$

Lemma 2. Let \mathfrak{U}_W be the uniform partition of $\Theta = [\underline{\theta}, \bar{\theta}]$ into W intervals each of diameter w

$$\begin{aligned} w &= \frac{\bar{\theta} - \underline{\theta}}{W} \\ \Theta_W^{(i)} &= [\underline{\theta} + (i-1)w, \underline{\theta} + iw], i = 1, \dots, W \\ \mathfrak{U}_W &= \{ \Theta_W^{(i)}, i = 1, \dots, W \}. \end{aligned}$$

and let $p^* \in \mathfrak{E}_{\mathfrak{L}}$, then

$$\mathbf{A}_{\mathfrak{U}_W}^p = 1 - \mathcal{O}(1/W)$$

Proof

Then by means of Theorem 5

$$\begin{aligned} d(\Theta_W^{(i)}) = \mathcal{O}(1/W) &\implies \mathfrak{h}(p^*(\Theta_W^{(i)}), P^*(\Theta_W^{(i)})) = \mathcal{O}(1/W) \\ &\implies d(P^*(\Theta_W^{(i)})) = \mathcal{O}(1/W), \quad \because p^* \in \mathfrak{E}_{\mathfrak{L}} \end{aligned}$$

Therefore

$$\sum_{i=1}^{|\mathfrak{U}_W|} \left(d(\Theta_W^{(i)}) \cdot P^*(\Theta_W^{(i)}) \right) = w \sum_{i=1}^W P^*([\underline{\theta} + (i-1)w, \underline{\theta} + iw]),$$

and we have

$$d(w \sum_{i=1}^W P^*(\Theta_W^{(i)})) = \mathcal{O}(1/W) \implies \mathbf{A}_{\mathfrak{U}_W}^p = 1 - \mathcal{O}(1/W)$$

Therefore the lower bound for the acceptance probability $\mathbf{A}_{\mathfrak{U}_W}^p$ of MRS approaches 1 no slower than linearly with the refinement of Θ by \mathfrak{U}_W . Note that this should hold for a general nonuniform partition with w replaced by the mesh. \square

References

1. von Neumann, J.: Various techniques used in connection with random digits. In: John Von Neumann, Collected Works. Volume V. Oxford University Press (1963)
2. Jones, G., Hobert, J.: Honest exploration of intractable probability distributions via markov chain monte carlo. *Statistical Science* **16**(4) (2001) 312–334
3. Mossel, E., Vigoda, E.: Phylogenetic MCMC algorithms are misleading on mixtures of trees. *Science* **309** (2005) 2207–2209
4. Moore, R.: Interval analysis. Prentice-Hall (1967)
5. Williams, D.: Weighing the Odds: A Course in Probability and Statistics. Cambridge University Press (2001)
6. Marsaglia, G.: Generating discrete random numbers in a computer. *Comm ACM* **6** (1963) 37–38
7. Walker, A.: An efficient method for generating discrete random variables with general distributions. *ACM Trans on Mathematical Software* **3** (1977) 253–256
8. Galassi, M., Davies, J., Theiler, J., Gough, B., Jungman, G., Booth, M., Rossi, F.: GNU Scientific Library Reference Manual - 2nd Ed. Network Theory Ltd. (2003)
9. Matsumoto, M., Nishimura, T.: Mersenne twister: A 623-dimensionally equidistributed uniform pseudo-random number generator. *ACM Trans. Model. Comput. Simul.* **8**(1) (1998) 3–30
10. Hofschuster, Krämer: C-XSC 2.0: A C++ library for extended scientific computing. In Alt, R., Frommer, A., Kearfott, R., Luther, W., eds.: Numerical software with result verification. Volume 2991 of Lecture notes in computer science. Springer-Verlag (2004) 15–35
11. Semple, C., Steel, M.: Phylogenetics. Oxford University Press (2003)
12. Jukes, T., Cantor, C.: Evolution of protein molecules. In Munro, H., ed.: Mammalian Protein Metabolism. New York Academic Press (1969) 21–32
13. Felsenstein, J.: Evolutionary trees from DNA sequences: a maximum likelihood approach. *Journal of Molecular Evolution* **17** (1981) 368–376
14. Sainudiin, R.: Machine Interval Experiments. pHD dissertation, Cornell University, Ithaca, New York (2005)
15. Brown, W., Prager, E., Wang, A., Wilson, A.: Mitochondrial DNA sequences of primates, tempo and mode of evolution. *Journal of Molecular Evolution* **18** (1982) 225–239
16. Hosten, S., Khetan, A., Sturmfels, B.: Solving the likelihood equations. *Found. Comput. Math.* **5**(4) (2005) 389–407
17. Casanellas, M., Garcia, L., Sullivant, S.: Catalog of small trees. In Pachter, L., Sturmfels, B., eds.: Algebraic statistics for computational biology. Cambridge University Press (2005) 291–304
18. Strimmer, K., von Haeseler, A.: Quartet puzzling: A quartet maximum likelihood method for reconstructing tree topologies. *Mol. Biol. Evol.* **13** (1996) 964–969
19. Levy, D., Yoshida, R., Pachter, L.: Beyond pairwise distances: Neighbor joining with phylogenetic diversity estimates. *Mol. Biol. Evol.* (Advance Access published on November 9, 2005)
20. Green, R., Krause, J., Ptak, S., Briggs, A., Ronan, M., Simons, J., Du, L., Egholm, M., Rothberg, J., Paunovic, M., Pääbo, S.: Analysis of onem million base pairs of neandertal DNA. *Nature* **444** (2006) 330–336
21. Hasegawa, M., Kishino, H., Yano, T.: Dating of the human-ape splitting by a molecular clock of mitochondrial dna. *Journal of Molecular Evolution* **22** (1985) 160–174

22. Efron, B., Halloran, E., Holmes, S.: Bootstrap confidence levels for phylogenetic trees. *Proceedings Natl. Acad. Sci.* **93** (1996) 13429–13429
23. Gilks, W., Wild, P.: Adaptive rejection sampling for Gibbs sampling. *Applied Statistics* **41** (1992) 337–348
24. Kulisch, U.: Advanced arithmetic for the digital computer, interval arithmetic revisited. In Kulisch, U., Lohner, R., Facius, A., eds.: *Perspectives on enclosure methods*. Springer-Verlag (2001) 50–70
25. Tucker, W.: *Auto-validating numerical methods*. Lecture notes, Uppsala University (2004)

List of Figures

1	19
2	20
3	21
4	22
5	23
6	24

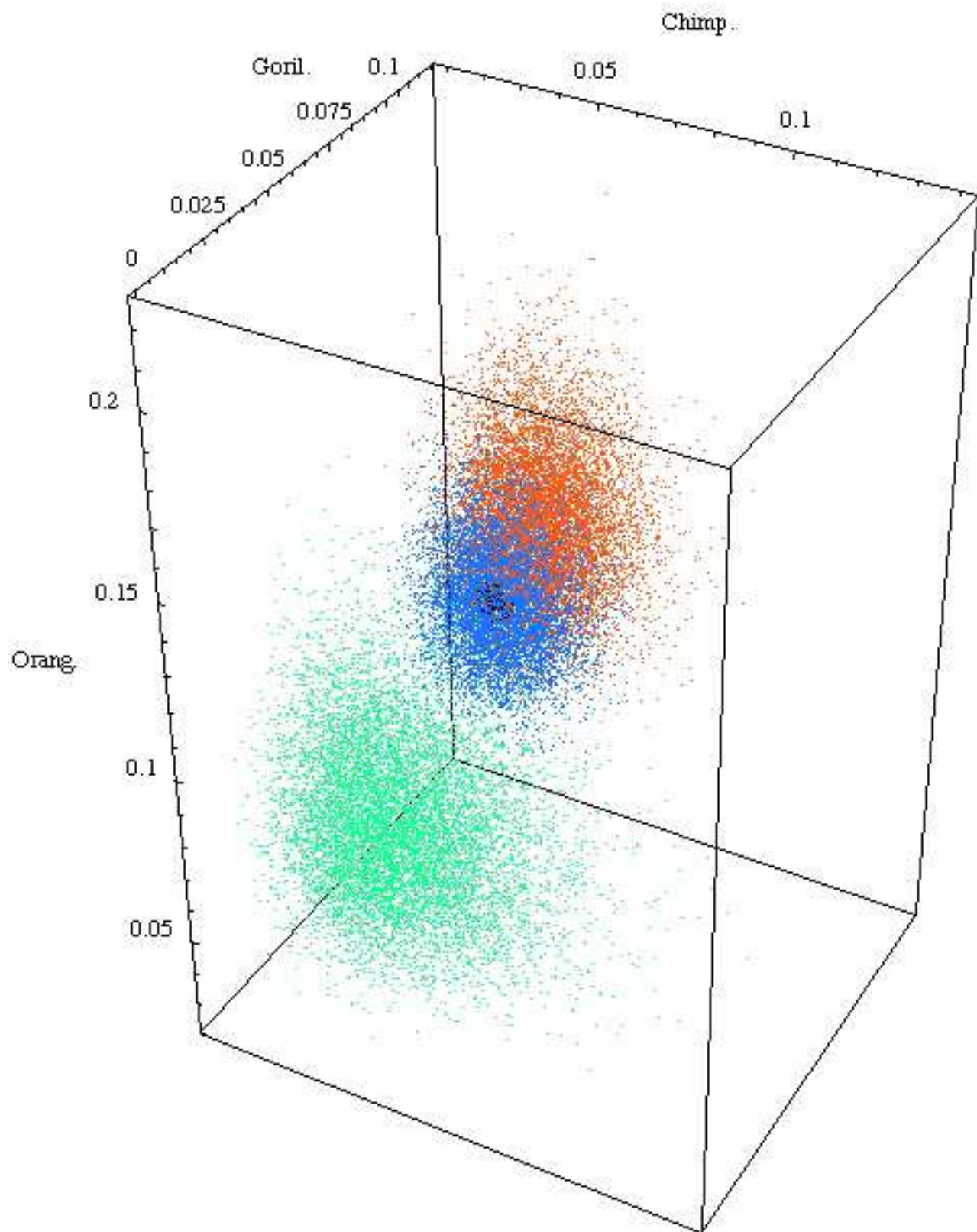


Fig. 1. 10000 Moore rejection samples from the posterior distribution over the three

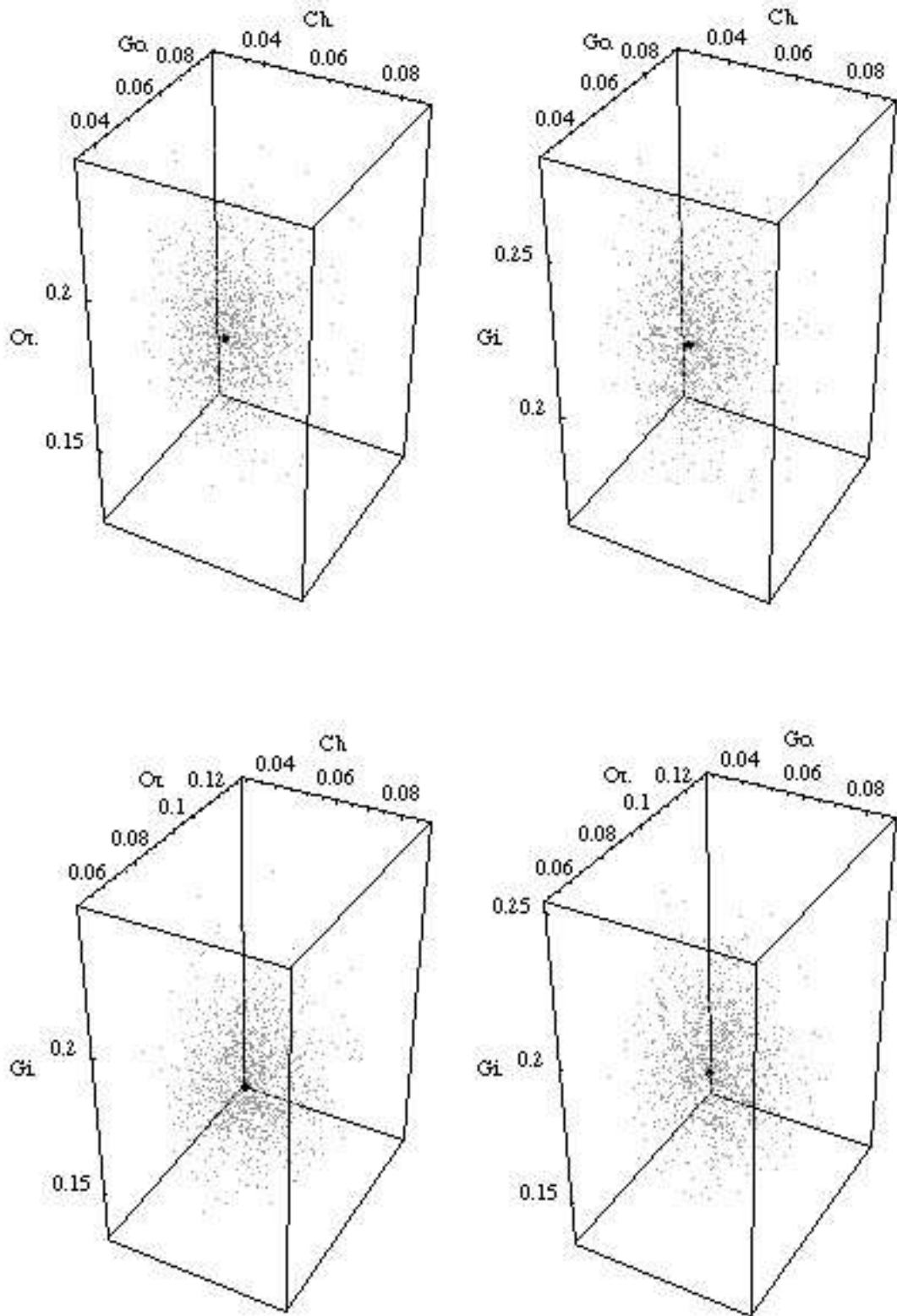


Fig. 2. 1000 Moore rejection samples (gray dots) from the posterior distribution over the unrooted quartet tree space of Chimpanzee (Ch.), Gorilla (Go.), Orangutan (Or.) and Gibbon (Gi.) plotted on the four species quartet tree space. The axes are

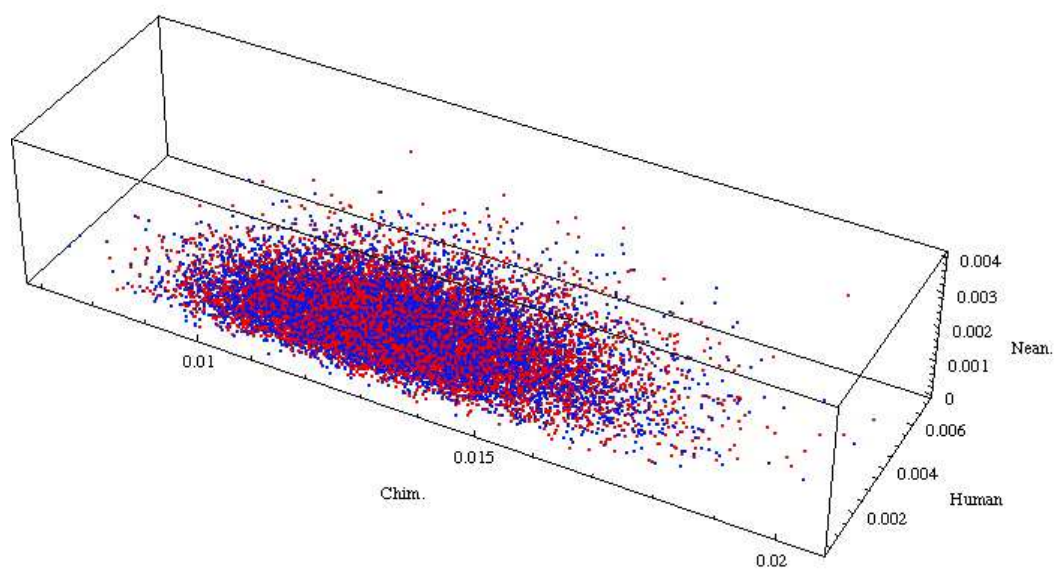


Fig. 3. 10000 Moore rejection samples each from the posterior distribution over the three branch lengths of the rooted phylogenetic tree space of Chimpanzee, Human and Neandertal under the Jukes-Cantor model (blue dots) and the HKY model (red dots)

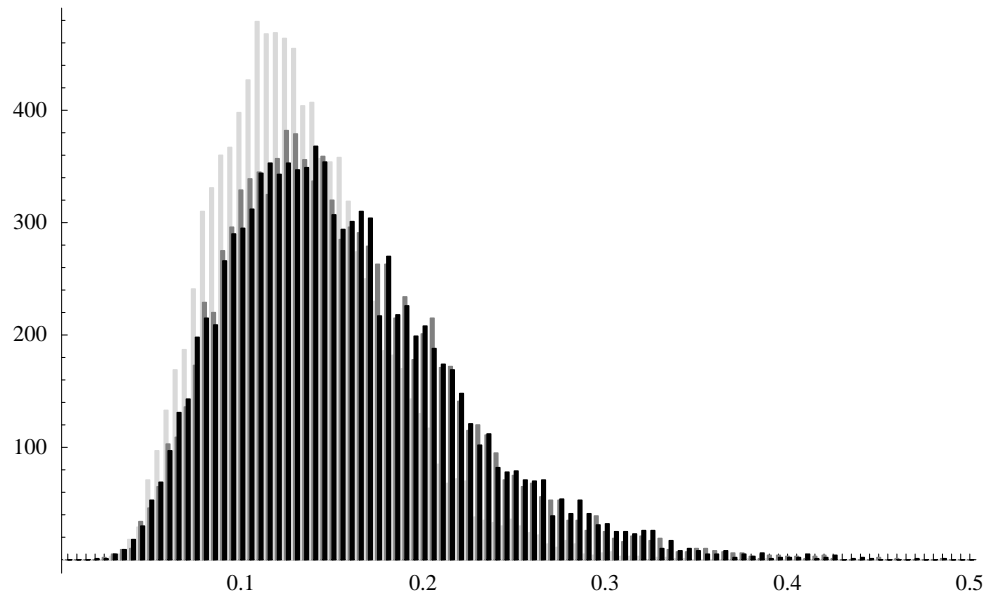


Fig. 4. Posterior distribution over the human-neandertal divergence time relative to the human-chimp divergence time based on 10000 independent samples from the (1) Midpoint-rooted tree estimates of the unrooted triplets under the Jukes-Cantor model (light gray), (2) rooted triplets under the Jukes-Cantor model (dark gray), and (3) rooted triplets under HKY model (black)

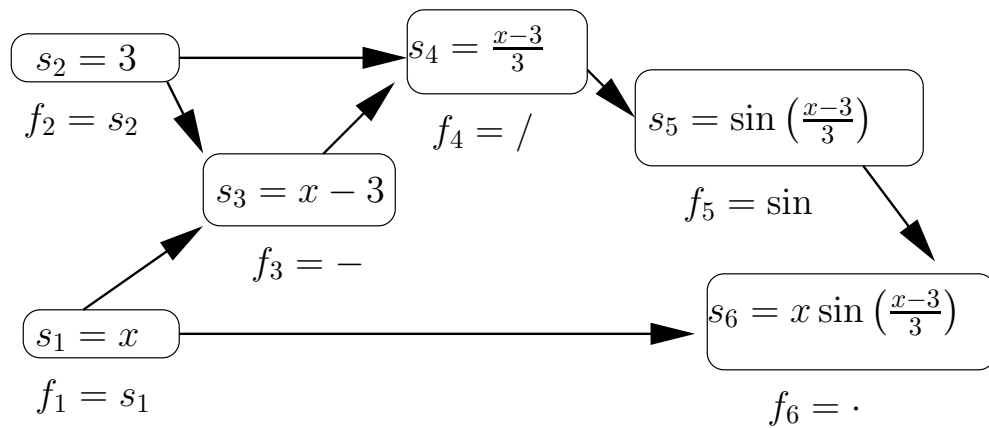


Fig. 5. Recursive evaluation of the sub-expressions f_1, \dots, f_6 on the DAG of the elementary function $f(x) = \odot f_6 = x \cdot \sin((x-3)/3)$

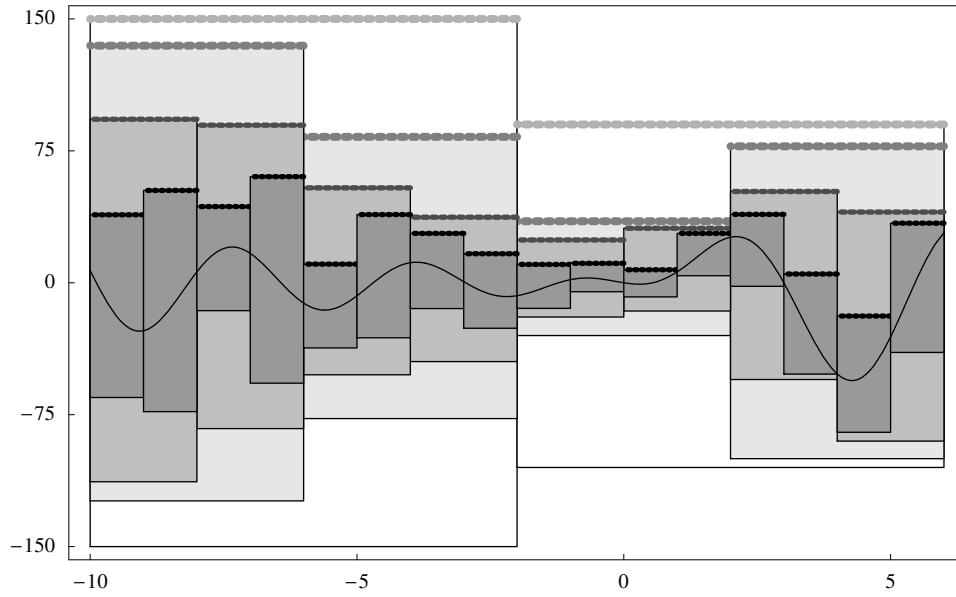


Fig. 6. Range enclosure of the interval extension of $-\sum_{k=1}^5 k x \sin\left(\frac{k(x-3)}{3}\right)$ linearly tightens with the mesh.